Boletim da Sociedade Astronômica Brasileira, **35**, no. 1, 99-103

Studying the Universe at High Redshift with GRBs

SFR and Chemical Enrichment

Gabriel Luiz Ferreira Santos & João Braga

[1] Instituto Nacional de Pesquisas Espaciais e-mail: gabriel.ferreira@inpe.br, joao.braga@inpe.br

Abstract. This work aims to perform a study of the chemical evolution of the interstellar medium of the host galaxies of events GRB 130606A and GRB 210905A and of the star formation rate (SFR) by counting GRBs. Therefore, the main goal of this work is to show how GRBs can be a very suitable tool to study some aspects of the Universe at high *redshifts*, since we obtained results that extend up to $z \sim 9$. Thus, we review the physical picture that is emerging of new constraints on reionization after several spectroscopic studies dedicated to obtaining observational data of GRBs at z > 6.

Resumo. Este trabalho tem como objetivo realizar um estudo da evolução química do meio interestelar das galáxias hospedeiras dos eventos GRB 130606A e GRB 210905A e da taxa de formação estelar (SFR) por meio da contagem de GRBs. Portanto, o principal objetivo deste trabalho é mostrar como os GRBs podem ser uma ferramenta muito adequada para estudar alguns aspectos do Universo em altos *redshifts*, uma vez que obtivemos resultados que se estendem até $z \sim 9$. Assim, revisamos o panorama físico que está surgindo de novas restrições à reionização após vários estudos espectroscópicos dedicados à obtenção de dados observacionais de GRBs com z > 6.

Keywords. GRBs – Reionization – Cosmology: observations

1. Introduction

The history of star formation and chemical evolution of the IGM is of intense interest to many in astrophysics, and it is natural to continue pushing the limit of observations to the earliest possible time, that is, to ever-higher *redshifts*. Our understanding of this history is increasing, with a consistent picture now emerging up to redshift $z \sim 13$ Robertson et al. (2023). Much current interest is in this frontier at high *redshifts*, where the first stars that may be responsible for the reionization of the Universe reside.

Although studies of the frontier at high star formation rate (SFR) *redshifts* have advanced rapidly, direct measurements beyond $z \sim 4$ remain difficult, as shown by significant divergences between different results. Gamma-ray bursts, due to their brightness and association with massive stars, offer an alternative to remedy such a situation, since the occurrence rate of long GRBs can be appropriately related to the SFR. *Swift* (Gehrels et al. 2004) satellite data reveal an increasing evolution in the rate of long GRBs relative to the SFR for intermediate *redshifts*; Taking this into account, we use the data from long GRBs of greater *redshift* to make a new determination of the SFR for $z > 4$.

In this sense, instead of obtaining the formation rate of massive stars from their observed populations, we directly measure the SFR through the mortality rate of massive stars, that is, the rate of occurrence of long GRBs, once their lifetimes are short (something on the order of a few million years).

The brightness of long GRBs spans a wide range of wavelengths, a fact that makes them ideal sources for measuring star formation history (SFH) (see the pioneering works of Totani (1997) and Wijers et al. (1998)). In recent years, the *Swift* satellite has increasingly increased the range of *redshifts* associated with long GRBs, including many events in $z \geq 4$. Surprisingly, the data show that the observations of long GRBs cannot be directly associated with the SFH, instead they imply some kind of further evolution (Daigne et al. (2006) and Kistler et al. (2008).

Furthermore, we used the luminosities of the long GRBs, estimated from the parameters T_{90} and E_{iso}, to exclude faint long GRBs that occurred at low *redshifts*, which would not be visible at our sample of high *redshifts*, that is, to compare "apples with apples". Although the statistics for long GRBs at high *redshifts* are relatively composed of a small sample of events, it allows a complementary approach to other SFR determinations Yüksel et al. (2008), which must deal with currently unknown extinction corrections, cosmic variance, and selection, most importantly, limited-flow surveys necessarily probe the brightest galaxies, which may contain only a small fraction of the star formation activity in the oldest epochs of the Universe.

Besides, after the burst of gamma-rays, there is a prolonged phase of radiation emission known as afterglow Xu et al. (2009). This phenomenon is the result of the interaction between the relativistic jet generated during the explosion and the surrounding environment.

Afterglow is produced mainly by two mechanisms: synchrotron emission and inverse Compton scattering. In synchrotron emission, relativistic electrons accelerated by the collision between the jet and interstellar gas emit radiation when deflected by magnetic fields Berger et al. (2005). This results in a wide range of radiation, from radio waves to X-rays. Inverse Compton scattering occurs when low-energy photons from the jet interact with high-energy electrons, extracting some of their energy. This results in an increase in the energy of the photons, changing their spectral distribution.

Therefore, when afterglow photons interact with gas and dust clouds in the ISM of the GRB host galaxy, a series of absorptions and scatterings occur so that we can probe the chemical properties of galaxies at high redshifts through spectroscopic analyzes of the photons of the afterglow that reach Earth Hartoog et al. (2015).

Consequently, this study focuses on harnessing GRBs as observational tools to unravel the mysteries of high-redshift astrophysics. Specifically, the research aims to elucidate the abundance of metallic ions and the stellar formation rates at high *redshift* Universe.

The pivotal data for this investigation originates from the ESO-VLT/X-SHOOTER instrument[1], which played a crucial role in capturing the spectra of the GRB 130606A and GRB 210905A events. Leveraging the remarkable capabilities of the ESO-VLT/X-SHOOTER, we conducted precise spectroscopic measurements to unravel the intricate details of these gamma-ray bursts. The instrument's high sensitivity and broad wavelength coverage proved instrumental in extracting rich information about the chemical composition of the Universe at high redshifts.

The observational data utilized for the determination of the SFR was sourced from the extensive database provided by the Swift satellite[2]. Leveraging its robust capabilities in capturing transient astrophysical events, Swift has been instrumental in collecting comprehensive multiwavelength data, crucial for assessing the SFR across cosmic epochs. The satellite's continuous monitoring and swift response to high-energy transients have significantly enriched our understanding of the evolving star formation processes within galaxies.

In Section 2, we present the model used to compute the SFR, the result and a comparison with another methods. In Section 3, we consider the spectra of GRB 130606A and GRB 210509A to study the chemical enrichment of their host galaxies, both at the end of EoR. Section 4 summarizes our conclusions.

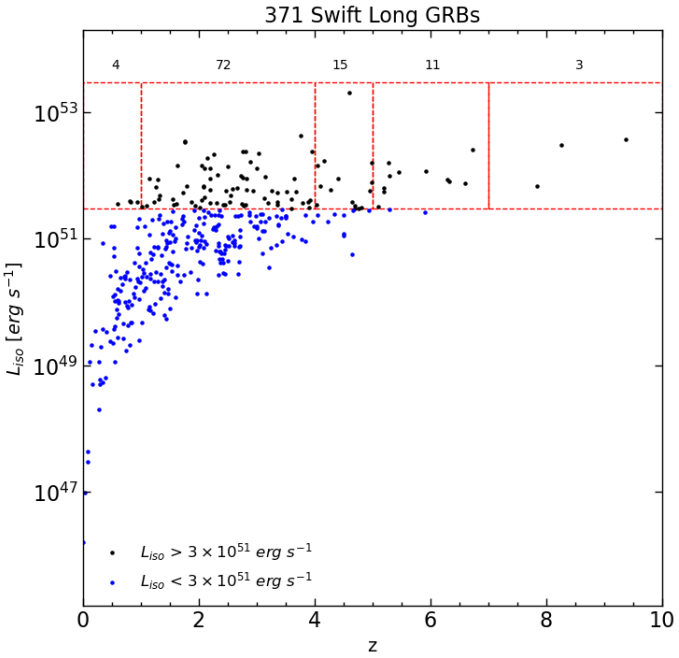

Figure 1. GRB sample from Swift database. The black dots represent the events selected for the study. They all have isotropic energy grater than $3 \times 10^{51}\ erg\ s^{-1}$.

2. SFR at high redshifts

Figure 1 presents a diagram that relates the isotropic energy and redshift of each GRB detected by Swift. Note that the events are organized into two populations based on the value of the isotropic energy. This was done to ensure that GRBs detected at low redshifts would also be observed if they had a higher redshift. Furthermore, the events were also separated according to redshift ranges so that we could write the SFR in terms of z after data analysis. The number of events present in each red box is above them. In total, 371 GRBs detected by Swift were analyzed.

Subsequently, we use the results of this event count as input data for the mathematical model that returns the SFR. Equation 1 summarizes the model used in this study. This model was proposed by Yüksel Yüksel et al. (2008). The idea is to calculate the average SFR over a given range of redshifts so that we are able to perform a functional fitting to obtain a curve that describes the evolution of SFR with redshift.

$$\langle \dot{\rho}_* \rangle_{z_1-z_2} = \frac{N^{obs}_{z_1-z_2}}{N^{obs}_{1-4}} \frac{\int_1^4 dz\, \dot{\rho}_*(z)(1+z)^{\alpha} \frac{dV/dz}{1+z}}{\int_{z_1}^{z_2} dz\, (1+z)^{\alpha} \frac{dV/dz}{1+z}}, \qquad (1)$$

where $N^{obs}_{z_1-z_2}$ is the expected number of GRBs with z between z_1 and z_2, N^{obs}_{1-4} is the number of events with z between 1 and 4, dV/dz is the comovel volume and α is a free parameter associated with the production efficiency of long GRBs in terms of redshift. According to Yüksel et al. (2008), $\alpha = 1.5$.

The function $\dot{\rho}_*(z)$ is the specific SFR for redshifts between 0 and 4. This function is determined using a fitting model based on Equation 2 and the dots are obtained using different methods for the SRF measurement, such as luminosity function or the strengh of spectral lines.

$$\dot{\rho}_*(z) = \dot{\rho}_0 \left[(1+z)^{a\eta} + \left(\frac{1+z}{B}\right)^{b\eta} + \left(\frac{1+z}{C}\right)^{c\eta} \right]^{1/\eta}, \qquad (2)$$

where

$$\begin{cases} a = 3.4 \\ b = -0.3 \\ c = -3.5 \\ B = 5000 \\ C = 9 \\ \eta = -10 \\ \dot{\rho}_0 = 0.02\ M_{\odot}\ yr^{-1}\ Mpc^{-3} \end{cases} \qquad (3)$$

It is also worth mentioning that the values of the coefficients B and C depend on the parameters a, b and c:

$$\begin{cases} B = (1+z_1)^{1-a/b} \\ C = (1+z_1)^{(b-a)/c}\ (1+z_2)^{1-b/c}. \end{cases} \qquad (4)$$

There is a general consensus on the fact that the long GRB rate does not strictly follow the SFR, but is actually enhanced by some unknown mechanisms at high redshifts. Several evolution scenarios have been considered to explain the observed increase, including the evolution of the rate density of long GRBs, cosmic evolution of metallicity, evolution of the stellar initial mass function, and evolution in the luminosity function. In short, there is much debate about the mechanisms responsible for such improvement.

With this, we were able to obtain 5 points for the specific SFR for $0 \leq z \leq 10$ and then perform the fitting using the same mathematical model as Equation 2. These results are present in the graph in Figure 2.

The values obtained in this work for the SFR based on counting GRBs in the interval $z \geq 4$ are greater than those obtained

[1] The reduced spectrum (FITS file) is available at the CDS via http://cdsarc.u-strasbg.fr/viz-bin/qcat?J/A+A/580/A139 and at https://archive.eso.org/wdb/wdb/eso/xshooter/form.

[2] Data available at https://cdsarc.cds.unistra.fr/viz-bin/cat/J/ApJS/248/21.

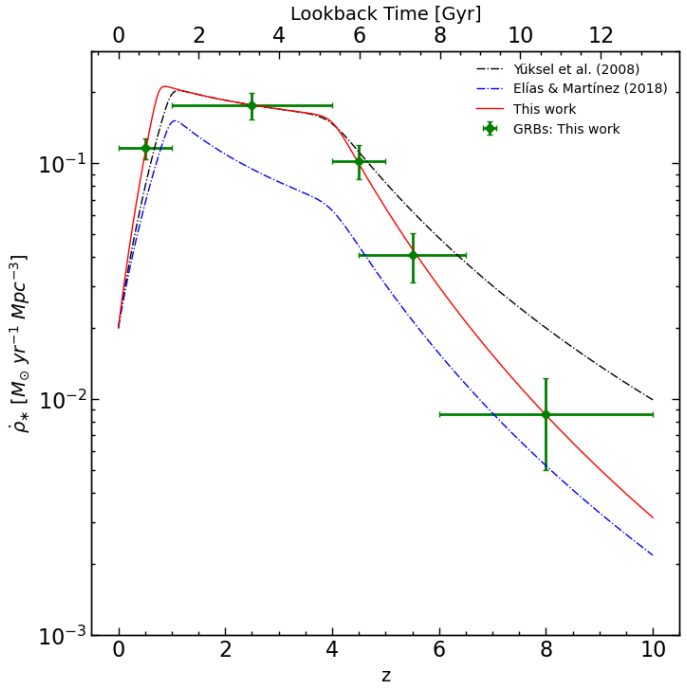

Figure 2. Specific SFR in terms of redshift, z, and lookback time. The black curve represents the results obtained by Yüksel et al. (2008) and the blue curve represents the adjustment performed by Elias et al. (2020). And the red curve reveals the adjustment made in this work with the most current data from the *Swift* Gehrels et al. (2004) satellite.

by Elias et al. (2020) and smaller than those derived by Yüksel et al. (2008). However, our results are in agreement with those of Wang et al. (2009). Still, the star formation rate derived in this work is higher than that estimated using the UV luminosity function of galaxies at high *redshifts*.

A significant population of low-luminosity star-forming galaxies that host GRBs may contribute to the increase in the observationally estimated SFR, since such galaxies are eventually not detected by other astronomical surveys. In this sense, research related to galaxy clusters via gravitational lensing, such as that of Richard et al. (2008), can help, as long as it is known how the cosmic variation occurs (in terms of *redshift*) of the quantities involved.

This helps to reconcile the differences between the results of this work and those obtained using other indicators of star formation. Yan et al. (2003) argue that the correction for the weak end of the UV luminosity function should be larger to take into account so-called dwarf galaxies which cannot be detected in astronomical surveys of LBGs. Therefore, since GRBs favor subluminous host galaxies Fynbo et al. (2003) Le Floc'h et al. (2003) Fruchter et al. (2006), such events offer the possibility of probing low-luminosity galaxies.

The Universe is completely ionized at $z \sim 6$ Wyithe et al. (2005) Fan et al. (2006), and it seems that the AGNs were not entirely responsible for such a Hopkins et al. (2008) process. According to Madau et al. (1999), the star formation density required to produce a sufficient ionizing photon flux is parameterized by two factors: the photon escape fraction (f_{esc}) and the IGM crowding (C). These parameters usually appear as a ratio, C/f_{esc}, which is not precisely known. For $C/f_{esc} \leq 30$, the SFR at $z = 6$ is $\dot{\rho}_*(z = 6) \geq 0.03\ M_\odot\ yr^{-1}\ Mpc^{-3}$, which corresponds with the results obtained in this work. It is worth noting that Yüksel et al. (2008) also obtained the same correspondence for the minimum star formation rate necessary to generate a completely reionized Universe at $z = 6$ from massive stars ($M \geq 20\ M_\odot$). Therefore, this finding is very interesting because in the same work, Madau et al. (1999), the authors state that for $z \geq 5$ the radiation emitted only by quasars would not be enough to ionize the IGM completely from $z \sim 3.6$.

3. Chemical abundances at the end of EoR

In the context of this work, we are interested in the Lyman spectral series[3]. This series involves electronic transitions where an electron jumps from a higher energy level to the fundamental level, that is, the lowest energy level allowed for the electron. This series is characterized by the emission or absorption of electromagnetic radiation in the ultraviolet region of the spectrum. In quantum terms, Lyman series transitions occur when the principal quantum number n of the electron decreases from a higher value to $n = 1$.

In particular, we are interested in the Lyman Alpha transition ($Ly\alpha$), in which electrons transit between the levels $n = 2$ and $n = 1$. Therefore, we expect to observe absorption lines in the *afterglow* spectrum of GRBs in the UV band. However, this transition can only be observed in this spectral range from the source's rest frame ($\lambda_\alpha = 121.57\ nm$). Therefore, we need to take into account the *redshift* of the GRB in question to determine the position of the $Ly\alpha$ absorption line in the spectrum. The equation that relates the rest wavelength of the source (λ_α) with the observed wavelength (λ) is given by:

$$\lambda = (1 + z_s)\,\lambda_\alpha, \tag{5}$$

where z_s is the *redshift* of the source (*source*).

The radiative flux must be modeled based on the optical depth associated with the $Ly\alpha$ absorption line. Therefore, the radiative energy flow is given by:

$$F(\lambda) = F_0\, e^{-\tau(\lambda)}, \tag{6}$$

where F_0 is a constant equal to the flux just before absorption occurs. This model was initially proposed by Miralda-Escudé (1998). The optical depth is given by:

$$\tau(\lambda) = \int_{z_s}^{z_n} \frac{\sigma(\omega)\, n(z)\, c}{(1 + z)\, H(z)}\, dz, \tag{7}$$

where $\sigma(\omega)$ is the photon absorption cross section $Ly\alpha$, $n(z) = n_0\ (1 + z)^3$ is the evolution of the hydrogen density of IGM with redshift, $H(z)$ is the Hubble parameter in terms of the redshift, $z_n = 6$ is the redshift associated with the end of EoR and c is the speed of light in vacuum. Note that n_0 is a free parameter used for the functional fitting.

Let's now define the δ parameter:

$$\delta = \frac{\Delta\lambda}{\lambda_\alpha(1 + z_s)} = \frac{\lambda - \lambda_\alpha(1 + z_s)}{\lambda_\alpha(1 + z_s)}$$

$$\delta = \frac{\lambda}{\lambda_\alpha(1 + z_s)} - 1. \tag{8}$$

We can write the ratio between the angular frequencies ω and ω_α as:

$$\frac{\omega}{\omega_\alpha} = \frac{(1 + z)}{(1 + z_s)(1 + \delta)}. \tag{9}$$

The difference between such angular frequencies is given by:

[3] EoR - Epoch of Reionization.

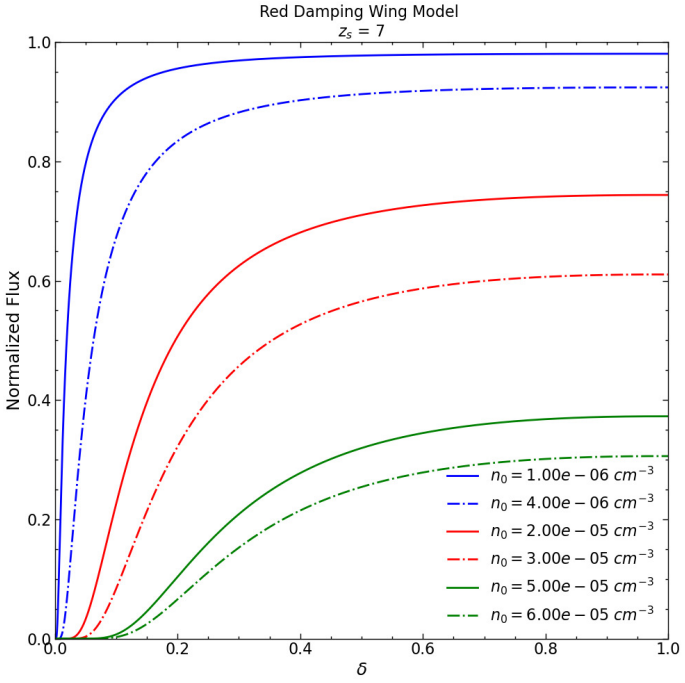

Figure 3. Curves obtained for Lyα absorption lines through the modeling discussed. The source is at $z_s = 7$ and each of the curves in the graph was generated for a given value of n_0.

$$\omega - \omega_\alpha = \left[\frac{(1+z)}{(1+z_s)(1+\delta)} - 1\right]\omega_\alpha. \tag{10}$$

With these expressions, we can write the cross section for photon absorption Lyα in terms of *redshift* (z), that is, in terms of the integration variable.

Therefore, after solving such an integral, we were able to make the graph shown in Figure 3. In Miralda-Escudé (1998), the researchers present the development of this model for the Lyα absorption line in more detail, which is also called *Red Damping Wing* (RDW).

Figure 3 presents the normalized flux diagram in terms of the δ parameter. Note that there is a series of Lyα absorption lines for a source at $z_s = 7$. Note that each line is associated with a specific n_0 value so that we can use it as a free fitting parameter.

The neutral hydrogen column density, that is, the number of neutral hydrogen atoms per unit area perpendicular to the line of sight, is given by:

$$N = \frac{c\, n_0}{H_0}\,(3.086{\times}10^{24}\ cm)\int_{z_n}^{z_s} dz\,\frac{(1+z)^2}{\left[\Omega_m(1+z)^3+\Omega_\Lambda\right]^{1/2}}. \tag{11}$$

Therefore, after obtaining the value of n_0 through the spectral fitting of the RDW, we can obtain the neutral hydrogen column density through Equation 11. The value for the neutral hydrogen column density is used in calculating the chemical abundance of metal ions.

Events GRB 130606A and GRB 210905A offer the opportunity for a direct application of the models discussed so far. The *afterglow* spectra of these GRBs were measured with X-SHOOTER, a medium-resolution spectrograph installed at the VLT in Cerro Paranal, in the Antofagasta region of Chile. The instrument operates in three spectral bands: UV; OPT and NIR. Furthermore, the X-SHOOTER is a UT3 Cassegrain focus-mounted spectrograph. It has three spectroscopic arms, each with optimized optics, dispersive elements and detectors.

The *Swift Burst Alert Telescope* (BAT) detected GRB 130606A on June 6, 2013 at 21:04:39 UT. The high-energy emission was extended, lasting $T_{90} = 277 \pm 19\ s$, firmly establishing GRB 130606A as a member of the long-lived GRB population. On the other hand, BAT detected GRB 210905A on September 5, 2021 at 00:12:41 UT. The duration of the initial gamma-ray burst was $T_{90} = 778 \pm 388\ s$, which also classifies GRB 210905A as a member of the long-lived GRB population.

Afterglow observations of GRB 130606A with the X-SHOOTER spectrograph mounted on ESO/VLT began at 03:57:41 UT on 7 June 2013. In contrast, *afterglow* observations of GRB 210905A began $\sim 2.53\ h$ (observer's reference frame) after the initial detection of the gamma ray burst, that is, at 02:44:29 on September 5, 2021.

There are other absorption lines very evident in each of the spectra. They are associated with the presence of metallic ions present in the ISMs of the host galaxies. Therefore, we selected chemical species whose spectral lines are in the instrument's wavelength range to probe their chemical abundance. The metallic ions are: C II; Fe II; N II; O III and Si III.

We define the chemical abundance parameter (or simply abundance parameter) as:

$$\varepsilon(X) = \log\left(\frac{n_X}{n_{HI}}\right) + 12, \tag{12}$$

where n_X is the numerical density of atoms of the element X and n_{HI} is the numerical density of neutral hydrogen atoms.

Therefore, it is clear that the ratio between n_X and n_{HI} is given by:

$$\frac{n_X}{n_{HI}} = \frac{N_X}{L}\,\frac{L}{N_{HI}} = \frac{N_X}{N_{HI}}, \tag{13}$$

where L is a characteristic length of the material medium.

Consequently, the abundance parameter in terms of the column densities of element X and neutral hydrogen is:

$$\varepsilon(X) = \log\left(\frac{N_X}{N_{HI}}\right) + 12. \tag{14}$$

The metallicity, [Fe/H], is defined based on $\varepsilon(X)$:

$$[\mathrm{Fe/H}] = \varepsilon(\mathrm{Fe}) - \varepsilon(\mathrm{Fe})_\odot, \tag{15}$$

where $\varepsilon(Fe)_\odot = 7.5$ is the solar abundance parameter for Iron.

Using 13 and 14, we can obtain the metallicity directly from the column density of Iron and neutral hydrogen:

$$[\mathrm{Fe/H}] = \log\left(\frac{N_{\mathrm{Fe}}}{N_{HI}}\right) + 4.5. \tag{16}$$

In this way, we can perform a chemical analysis of the host galaxies of the GRB 130606A and GRB 210905A events using the spectra measured with X-SHOOTER. The first step is to identify the absorption lines of the metal ions of interest. Next, we need to fit a Gaussian to measure the equivalent width of the line. Finally, simply calculate the column density of the ion in question using the following relationship Chornock et al. (2013):

$$\log(N_X) = 1.23 \times 10^{20}\ cm^{-2}\,\frac{EW}{\lambda^2 f_{ij}}, \tag{17}$$

where EW is the equivalent width of the line in angstrom, λ is the wavelength of the transition in the rest frame also in angstrom and f_{ij} is the oscillator strength of the transition.

Table 1. Column density of metal ions and their respective abundance parameters for the host galaxy of GRB 130606A at $z \sim 6$.

Ion	$\log(N_X)$ $[cm^{-2}]$	ε
Fe II	12,66	4,71
C II	12,81	4,86
N II	13,08	5,13
O III	16,09	8,14
Si III	13,39	5,44

Table 2. Column density of metal ions and their respective abundance parameters for the host galaxy of GRB 210905A at $z \sim 6.32$.

Ion	$\log(N_X)$ $[cm^{-2}]$	ε
Fe II	12,32	2,34
C II	13,72	3,74
N II	13,28	3,30
O III	13,66	3,68
Si III	13,61	3,63

The values of f_{ij} as well as the rest wavelengths of the transitions studied here were taken from the NIST website (*National Institute of Standards and Technology*)[4].

Tables 1 and 2 present the results of the abundance parameters measured for GRB 130606A and GRB 210905A, respectively. We can use the Fe II abundance parameters and the Equation 15 to calculate the metallicities of the host galaxies of the events. Therefore, for the host galaxies of the GRB 130606A and GRB 130606A events, respectively, we have:

$$[\text{Fe/H}] = -2.79 \tag{18}$$

and

$$[\text{Fe/H}] = -5.16. \tag{19}$$

4. Conclusions

GRBs offer an alternative way to study the high-redshift Universe due to their intense luminosity. In particular, we were able to determine chemical enrichment and metallicity for two galaxies at the end of the EoR by using GRB spectra from events GRB 130606A and GRB 210905A. The results are in good agreement with other works (see Chornock et al. (2013) and Saccardi et al. (2023)). Implications for the EoR: The Universe is fully ionized at $z \sim 6$. AGNs are not the main source of ionizing photons, so massive stars play an important role in explaining this state of ionization. Our SFR results for massive stars are capable of reproducing a fully ionized Universe at $z \sim 6$ ($SFR \geq 0.03 M_\odot\, yr^{-1}\, Mpc^{-3}$) (see Madau et al. (1999)). Therefore, GRBs can be used to study the Universe up to $z \sim 20$ due to their high luminosity ($L \sim 10^{51} erg\ s^{-1}$), allowing us to obtain data not only from the EoR but also from a Universe less than 400,000 years old (see Ciardi et al. (2000)).

Acknowledgements. I would like to thank capes for the financial support.

References

Berger, E., et al. 2005, ApJ, 634, 501
Ciardi, B., Loeb, A. 2000, ApJ, 540, 687
Chornock, R., et al. 2013, ApJ, 774, 26
Daigne, F., Rossi, E. M., Mochkovitch, R. 2006, MNRAS, 372, 1034
Elías-Chávez, M., Martínez, O. M. 2020, arXiv preprint arXiv:2006.03367
Fan, X., et al. 2006, ApJ, 132, 117
Fruchter, A. S., et al. 2006, Nature, 441, 463
Fynbo, J. U., et al. 2003, AA, 406, L63
Gehrels, N., et al. 2004, ApJ, 611, 1005
Hartoog, O. E., et al. 2015, AA, 580, A139
Hopkins, P. F., et al. 2008, ApJ, 175, 356
Kistler, M. D., et al. 2008, ApJ, 673, L119
Le Floc'h, E., et al. 2003, AA, 400, 499
Madau, P., Haardt, F., Rees, M. J. 1999, ApJ, 514, 648
Miralda-Escudé, J. 1998, ApJ, 501, 15
Van Paradijs, J., Kouveliotou, C., Wijers, R. A. M. J. 2000, ARAA, 38, 379
Richard, J., et al. 2008, ApJ, 685, 705
Robertson, B. E., et al. 2023, Nature, 7, 611
Salvaterra, R., Chincarini, G. 2007, ApJ, 656, L49
Saccardi, A., et al. 2023, AA, 671, A84
Totani, T. 1997, ApJ, 486, L71
Wang, F. Y., Dai, Z. G. 2009, MNRAS, 400, L10
Wijers, R. A. M. J., et al. 1998, MNRAS, 294, L13
Wyithe, J. S. B., Loeb, A., Carilli, C. 2005, ApJ, 628, 575
Yan, H., Windhorst, R. A. 2003, ApJ, 600, L1
Yüksel, H., et al. 2008, ApJ, 683, L5
Xu, Z., Wei, D. M. 2009, Sci China G, 52, 1428

[4] `https://physics.nist.gov/PhysRefData/ASD/lines_form.html`